IOP Publishing New J. Phys. 26 (2024) 043021 https://doi.org/10.1088/1367-2630/ad3ea8

New Journal of Physics
The open access journal at the forefront of physics

Deutsche Physikalische Gesellschaft DPG
IOP Institute of Physics

Published in partnership with: Deutsche Physikalische Gesellschaft and the Institute of Physics

OPEN ACCESS

RECEIVED
24 January 2024

REVISED
10 April 2024

ACCEPTED FOR PUBLICATION
15 April 2024

PUBLISHED
26 April 2024

PAPER

Measurement of infrared magic wavelength for an all-optical trapping of $^{40}Ca^{+}$ ion clock

Yao Huang[1,2], Miao Wang[1,2], Zheng Chen[1,2,3], Chengbin Li[1,2,*], Huaqing Zhang[1,2], Baolin Zhang[1,2], Liyan Tang[1,2], Tingyun Shi[1,2], Hua Guan[1,2,4,*] and Ke-Lin Gao[1,2,*]

[1] State Key Laboratory of Magnetic Resonance and Atomic and Molecular Physics, Innovation Academy for Precision Measurement Science and Technology, Chinese Academy of Sciences, Wuhan 430071, People's Republic of China
[2] Key Laboratory of Atomic Frequency Standards, Innovation Academy for Precision Measurement Science and Technology, Chinese Academy of Sciences, Wuhan 430071, People's Republic of China
[3] School of Physical Sciences, University of Chinese Academy of Sciences, Beijing 100049, People's Republic of China
[4] Wuhan Institute of Quantum Technology, Wuhan 430206, People's Republic of China
* Authors to whom any correspondence should be addressed.

E-mail: cbli@apm.ac.cn, guanhua@apm.ac.cn and klgao@apm.ac.cn

Keywords: magic wavelength, optical clock, static polarizability, all-optical trapping

Abstract

For the first time, we experimentally determine the infrared magic wavelength for the $^{40}Ca^{+}$ $4s^2S_{1/2} \rightarrow 3d^2D_{5/2}$ electric quadrupole transition by observation of the light shift canceling in $^{40}Ca^{+}$ optical clock. A 'magic' magnetic field direction is chosen to make the magic wavelength insensitive to both the linear polarization purity and the polarization direction of the laser. The determined magic wavelength for this transition is 1056.37(9) nm, which is not only in good agreement with theoretical predictions ('Dirac–Fock plus core polarization' method) but also more precise by a factor of about 300. Using this measured magic wavelength, we also derive the differential static polarizability to be −44.32(32) a.u., which will be an important input for the evaluation of the blackbody radiation shift at room temperatures. Our work paves a way for all-optical-trapping of $^{40}Ca^{+}$ optical clock.

1. Introduction

With rapid development of laser technology, state-of-the-art optical clocks have now reached an accuracy or frequency stability at the level of 10^{-18} [1–6] or higher [7, 8], which is two orders of magnitude better than the state-of-the-art microwave atomic clocks. At this level of accuracy, optical clocks can play a critical role in redefining the second [9], in searching for variation of fundamental constants [10–13], and in chronometric leveling [14]. For many neutral-atom optical lattice clocks [4, 5], the ac Stark shift due to black body radiation (BBR) or lattice lasers can be a limiting factor for achieving such high accuracy; for ion-based clocks, on the other hand, micromotion shifts may limit the accuracy of some clocks [2, 7]. One way to reduce the micromotion shifts is to apply the all-optical trapping technique [15–17], where the micromotion shift will be gone when the radio-frequency (RF) field is switched off. Since the laser used for all-optical trapping can be chosen at a magic wavelength [18–21], the energy shift in the relevant transition will be zero and thus the trapping potential will introduce no shift in the clock transition frequency. Therefore, for a magic-wavelength optical-trapped ion, both the micromotion and ac Stark shift can be greatly suppressed. In addition to the accuracy of a clock, the frequency stability is also a very important issue when evaluating a clock. Comparing to neutral-atom lattice clocks, the stability of a single ion clock is limited by the quantum projection noise limit for ion number N is only one. Recently, the optical trapping of Coulomb ion crystals has been demonstrated [22], which sheds light on the development of all-optical trapping ion clocks using multiple ions to achieve a better frequency stability.

Precision measurements of magic wavelengths in atoms are also very important in fundamental studies of atomic structure. For example, a measurement of line strength ratio by magic wavelength can bring a new perspective for determining accurate transition matrix elements, which are important in testing atomic

computational methods and in interpreting atomic parity non-conservation [23–25]. Precision measurements of magic wavelengths in ions can be used to derive relevant oscillator strengths and polarizabilities for clock states [26], which is essential for evaluating the BBR shift on the 10^{-18} level at room temperatures.

The magic wavelengths of $^{40}Ca^{+}$ have recently been studied both theoretically [27–29] and experimentally [26]. Two magic wavelengths for the $4s_{1/2} \rightarrow 3d_{5/2}$ ($m_J = 1/2, 3/2$) clock transitions near 395.79 nm have been measured to high accuracy, which are in well agreement with all existing theoretical predictions. However, these magic wavelengths are very close to the $4s_{1/2} \rightarrow 4p_{3/2}$ and $4s_{1/2} \rightarrow 4p_{1/2}$ resonant transitions. The near resonant light has high spontaneous photon scattering rates that can result in a severe heating process [30]. Thus, these magic wavelengths are not ideal choices for the optical trapping of ions. Therefore, in order to achieve optical trapping of ions, it is important to search for magic wavelengths far off any resonant transitions; for $^{40}Ca^{+}$ in particular, magic wavelengths in the infrared region are desirable.

In this letter, we will report the experimental measurement of an infrared magic wavelength by observation of the light shift canceling in $^{40}Ca^{+}$ optical clock. The clock has an uncertainty of 2.2×10^{-17} [31]. The clock is suitable for making a differential measurement, the clock uncertainty would only introduce a negligible measurement uncertainty of <0.01 nm. We will present a method to extract a reduced transition matrix element using our measured magic wavelength. We will also determine a static differential polarizability that is an important parameter in evaluating the BBR shift at room temperatures.

2. Experimental measurement

Calculating or measuring an infrared magic wavelength is very different from measuring an ultraviolet magic wavelength [26]. Briefly speaking, in theoretical calculation, the predicted magic wavelengths have much larger uncertainty compared to the ultraviolet magic wavelengths. Several theoretical works also show that the orientations of magnetic field, laser propagation, and laser polarization will have effects on the magic wavelengths of the $4s^2S_{1/2} \rightarrow 3d^2D_{5/2}$ transition in $^{40}Ca^{+}$ [27–29, 32]. For measuring an infrared magic wavelength, however, we need to carefully control the laser and magnetic field configurations and carefully evaluate systematic shifts.

2.1. Experimental setup

As illustrated in figure 1, to setup the experiment, first of all, a single $^{40}Ca^{+}$ ion is trapped in a miniature ring Paul trap and laser cooled to the temperature of a few mK. To measure the magic wavelength, the clock laser is locked to the Zeeman components of clock transition and the light shift on the clock transition can be observed by switching on and off the laser with wavelength around 1050 nm (named L_m laser for short in the following sections). Detailed schematic diagram of the experimental sequence can be found in figure 7 in the appendix A. To keep the L_m laser linearly polarized during the measurement, a polarizer (Glan–Tyler Prism) is placed in the light path before ion–light interaction takes place. In doing so, the linear polarization purity can reach >99%, which can be derived by analyzing the incident and transmission lights of L_m laser. The wavelength of the L_m laser used in the experiment is measured with a precision of 100 MHz by a wavelength meter (WS-7, HighFinesse GmbH) which is calibrated by $^{40}Ca^{+}$ ion's clock laser 729 nm and a femtosecond optical frequency comb referenced to International System of Units (SI) second via Global Positioning System (GPS), the accuracy of the measurement is then expected to be <100 MHz or <0.2 pm. The power of L_m laser is measured using a commercial power meter (S120VC, Thorlabs Inc.) with a power variation within 5%. To increase the measurement accuracy, a 'magic' magnetic field direction is chosen to make the magic wavelength insensitive to both the linear polarization purity and the polarization direction of the laser.

2.2. Ac Stark shift

The ac Stark shift caused by a laser can be written in the form [32]

$$\Delta E_i = -\frac{F^2}{2}\alpha_i(\omega) \tag{1}$$

$$\alpha_i(\omega) = \alpha_i^{S}(\omega) + A\cos\theta_k \frac{m_J}{2J}\alpha_i^{V}(\omega) + \frac{3\cos^2\theta_p - 1}{2} \cdot \frac{3m_J^2 - J(J+1)}{J(2J-1)}\alpha_i^{T}(\omega) \tag{2}$$

where F is the strength of the ac electromagnetic field, $\alpha_i^{S}(\omega)$ [33], $\alpha_i^{V}(\omega)$ [34], and $\alpha_i^{T}(\omega)$ [35] are, respectively, the scalar, the vector, and the tensor polarizabilities for quantum state i at frequency ω. Also, m_J and J are respectively the magnetic quantum number and total azimuthal quantum number of state i. For the $^{40}Ca^{+}$ ion's clock transition $4s^2S_{1/2} \rightarrow 3d^2D_{5/2}$, i represents the energy level state $4s^2S_{1/2}$ or $3d^2D_{5/2}$; $m_J = \pm 1/2$ for state $4s^2S_{1/2}$, $m_J = \pm 1/2, \pm 3/2, \pm 5/2$ for state $3d^2D_{5/2}$; and $J = 1/2$ for state $4s^2S_{1/2}$, $J = 5/2$

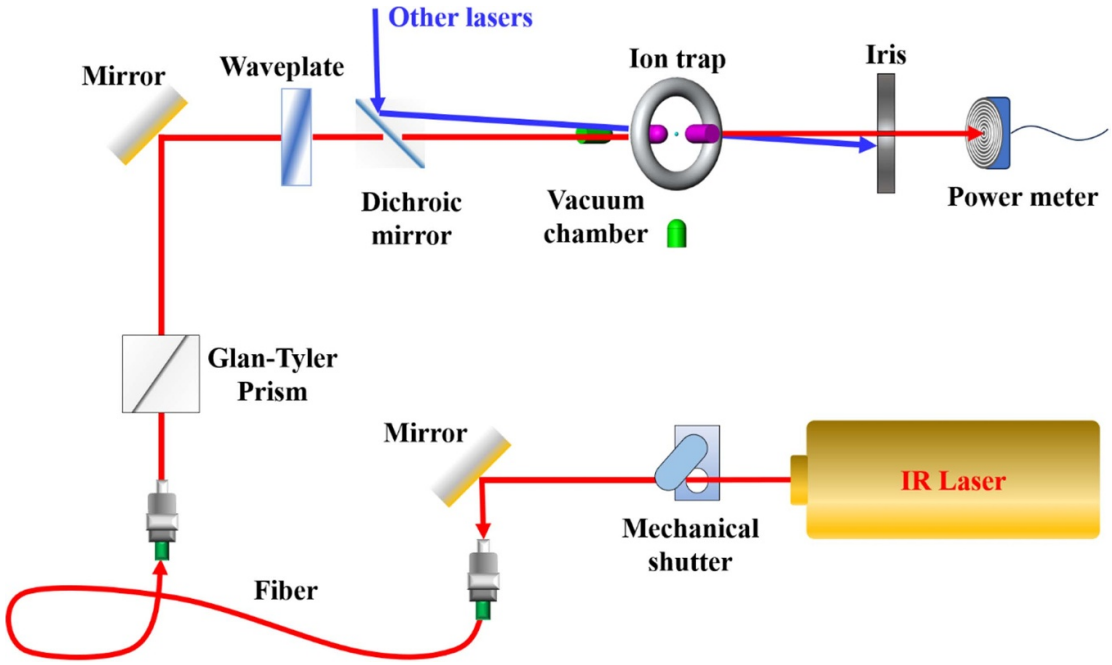

Figure 1. Schematic diagram for the measurement of the infrared magic wavelength.

for state $3d^2D_{5/2}$. The tensor component $\alpha_i^{\mathrm{T}}(\omega)$ will be taken into account only when $J > 1/2$ [35]. In equation (2), the laser polarization A represents the degree of polarization: in particular, $A = 0$ corresponds to linear polarization, while $A = +1$ (or -1) corresponds to right- (or left-) circular polarization. And the exact definition of A is given in [32]. The angle θ_k between the laser propagation direction $\hat{k}$ and the magnetic field direction $\hat{B}$, the angle θ_{p} between the laser polarization direction and $\hat{B}$ are all important parameters affecting the ac Stark shift. In previous theoretical calculations [27–29], $A = 0$ and $\cos\theta_{\mathrm{p}} = 1$ were chosen when calculating the polarizabilities and extracting the magic wavelengths under a linearly polarized laser field.

We first consider the case where $A = 0$ and $\cos\theta_{\mathrm{p}} = 1$ in our experiment. Unlike the 395 nm magic wavelength measurement [26], it is found that the magic wavelength here is very sensitive to the parameters A, θ_k, and θ_{p}. Thus, we have to make sure to control these parameters to be very stable and precise. The parameter A is measured to be 0.005(5) that corresponds to an almost linear polarization, but the $A\cos\theta_k$ term still affects the measurement because the ac Stark shifts to the sublevels $m_J = -3/2$ and $m_J = 3/2$ are found to be different. Setting $\cos\theta_k$ to be 0 will lower the effect caused by the polarization impurity.

In the experimental setup, the L_{m} laser polarization and propagation directions are kept unchanged. In the beginning of our measurement, the background magnetic field of the ion is compensated to 0 by adjusting the currents in the three pairs of Helmholtz coils. The magnetic field amplitude can be measured by observing the clock transition Zeeman components. By adjusting the currents in the coils, the relationship between the current in each pair of coils and the magnetic field it produces is measured. By changing the currents in the coils, one can produce the magnetic field of any direction while keeping the amplitude constant. In the end of our measurement, the compensated background magnetic field is measured again so that the background magnetic field drift amplitude can be evaluated.

2.3. Measurement result

To measure the magic wavelength λ_{m}, we have studied ac Stark shift within a few nanometers around λ_{m}. As shown in figure 2, we have measured the averaged ac Stark shifts of the two Zeeman transitions: $|4s^2S_{1/2},\ +1/2\rangle \rightarrow |3d^2D_{5/2},\ +3/2\rangle$ and $|4s^2S_{1/2},\ -1/2\rangle \rightarrow |3d^2D_{5/2},\ -3/2\rangle$ at six wavelengths of L_{m} laser, each being measured for about 2000 s. Then the six points were fitted linearly and the magic wavelength was obtained. Ac Stark shift measurements are made with five different L_{m} laser power (different colors in figure 2), no obvious magic wavelength change can be observed. Evaluation of systematic shifts is of great importance in the measurement of the infrared magic wavelength since it is sensitive to the above-mentioned parameters. The systematic shifts caused by the uncertainties in θ_k and θ_{p}, by the laser power, by the broadband laser spectrum (with impure portion of the laser wavelength), and by the background magnetic field drift have also been evaluated.

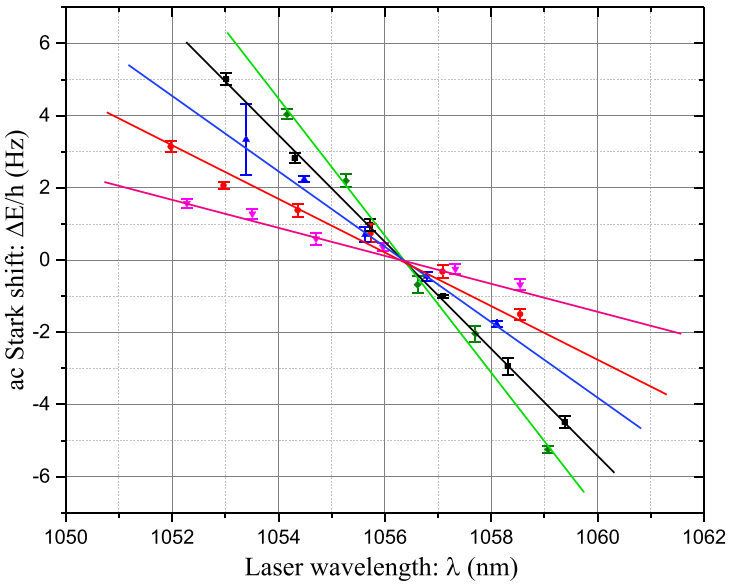

Figure 2. Ac Stark shift as a function of laser wavelength at different L_{m} laser power. Green symbol: 25 mW; black symbol: 20 mW; blue symbol: 15 mW; red symbol: 10 mW; purple symbol: 5 mW. The lines are the linear fits to the data points with the same color accordingly. The measured ac Stark shift and magic wavelength correspond to average of the two Zeeman transitions: $|4s^2S_{1/2},\ +1/2\rangle \rightarrow |3d^2D_{5/2},\ +3/2\rangle$ and $|4s^2S_{1/2},\ -1/2\rangle \rightarrow |3d^2D_{5/2},\ -3/2\rangle$.

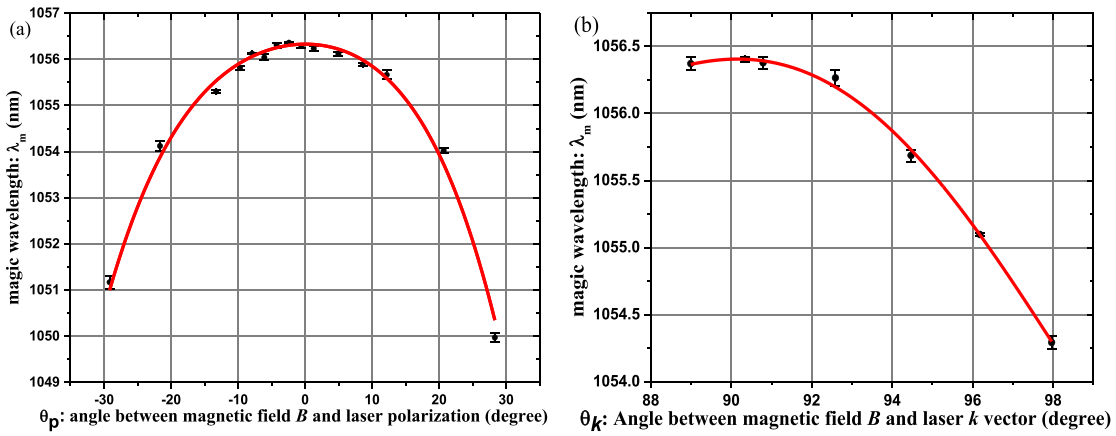

Figure 3. (a) The magic wavelength as a function of θ_{p} (the angle between magnetic field direction and the laser polarization) when $\theta_k = 90°$; (b) The magic wavelength as a function of θ_k (the angle between magnetic field direction and the laser propagation direction) when $\theta_{\mathrm{p}} = 0°$. The measured ac Stark shift and magic wavelength correspond to the Zeeman transition $|4s^2S_{1/2},\ -1/2\rangle \rightarrow |3d^2D_{5/2},\ -3/2\rangle$. Each data point shows the average of an experiment lasts for 1–4 h. The error bars only include the statistical errors, yet the systematic errors caused by the magnetic field drifting, the laser power drifting, and the laser pointing drifting are not included. The fitted solid curve is a polynomial fit of the data set to the 4th order.

For estimating the systematic shift due to θ_{p}, we scanned θ_{p} from $-30°$ to $30°$. We found that the measured magic wavelength of the Zeeman transition $|4s^2S_{1/2},\ -1/2\rangle \rightarrow |3d^2D_{5/2},\ -3/2\rangle$ became longer when θ_{p} was near $0°$, as observed in [28], and shown in figure 3(a). Experimentally we can change θ_{p} until the measured magic wavelength becomes the longest. According to the precision of θ_{p} of $\sim$1 degree that we can experimentally have, θ_{p} could cause a measurement uncertainty of 0.03 nm. However, for reasons such as the viewports that would change the polarization slightly, we can still see strong effects caused by A. Practically, the magnetic field direction can be adjusted to make $\cos\theta_k = 0$. As shown in figure 3(b), when measuring the magic wavelength difference between the two Zeeman transitions: $|4s^2S_{1/2},\ +1/2\rangle \rightarrow |3d^2D_{5/2},\ +3/2\rangle$ and $|4s^2S_{1/2},\ -1/2\rangle \rightarrow |3d^2D_{5/2},\ -3/2\rangle$, we found that this difference came to 0 when $\theta_k = 90°$, as shown in figure 4, indicating that the $A\cos\theta_k$ term no longer contributed to the systematic shift for the level of 0.001 43 nm. Experimentally we can change θ_k until the measured magic wavelength difference between the two Zeeman transitions above becomes 0. The experimental precision of θ_k of $\sim$1 degree would cause a measurement uncertainty for the measured magic wavelength of 0.01 nm.

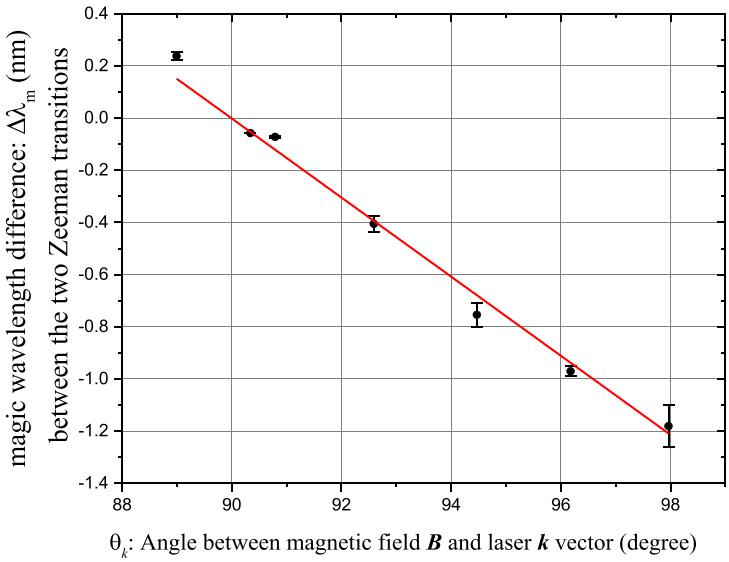

Figure 4. The magic wavelength difference between the two Zeeman transitions $|4s^2S_{1/2},\ +1/2\rangle \rightarrow |3d^2D_{5/2},\ +3/2\rangle$ and $|4s^2S_{1/2},\ -1/2\rangle \rightarrow |3d^2D_{5/2},\ -3/2\rangle$ as a function of θ_k. When θ_k is closer to 90°, the measured magic wavelength difference between the two Zeeman transitions comes to ∼0.

Table 1. Uncertainty budget for the infrared magic wavelength measurement. Effects with both shift and uncertainty smaller than 0.001 nm are not listed. Units in table are nm.

Source	Shift	Uncertainty
Statistical	—	0.02
θ_p	0	0.03
θ_k	0	0.01
Laser power	−0.03	0.03
Broadband laser spectrum	0.005	0.005
Background magnetic field shift	0	0.08
Total uncertainty	−0.04	0.09
Magic wavelength with correction	1056.37(9)	

Table 2. Comparison of the infrared magic wavelength and the $^{40}Ca^+$ blackbody radiation shift (Hz) at 300 K. Units in table are nm.

		Theoretical work	
	This work (experiment)	All-order method	DFCP method
Magic wavelength	1056.37(9)	1052.26 [27]	1074(26) [29] 1074(32) [28]
BBR shift	0.3816(28)	0.3811(44) [36] 0.31(1) [40]	0.380(14) [41] 0.368 [42]

2.4. Systematic error budget

The background magnetic field may be changing during the measurement. Since the measurement was found to be sensitive to the magnetic field direction, the effects of magnetic field change should be considered. By measuring the compensated magnetic field amplitude (which should be about 0) every few hours, the background magnetic field would only be changed by less than 30 nT during the whole experiment. Since the applied magnetic field amplitude is 3800 nT, we estimated that both θ_p and θ_k would gain an uncertainty of less than 0.5° due to the background magnetic field change. According to the relationship between the magic wavelength and those parameters, magnetic field change during the whole experiment would cause a magic wavelength measurement uncertainty of 0.08 nm.

Table 1 lists the systematic error budget. Details about the systematic shift evaluation can be found in the appendix B.

With the corrections shown in table 1, the infrared magic wavelength for the two Zeeman transitions $|4s^2S_{1/2},\ +1/2\rangle \rightarrow |3d^2D_{5/2},\ +3/2\rangle$ and $|4s^2S_{1/2},\ -1/2\rangle \rightarrow |3d^2D_{5/2},\ -3/2\rangle$ is determined as 1056.37(9) nm. To date, there are a few theoretical calculations on this wavelength [27–29], as listed in table 2 in section 3. One can see that our result is in fairly good agreement with these calculations but with much smaller uncertainty.

3. Result calculation and evaluation

3.1. Dynamic polarizability

Theoretically, using the perturbation theory, the dynamic electric dipole polarizabilities of a given atomic state can be expressed as [33]

$$\alpha_i^{\mathrm{S}}(\omega) = \frac{2}{3(2J_i+1)} \sum_k \frac{\Delta E_{ki} |\langle \Psi_i \| D \| \Psi_k \rangle|^2}{\Delta E_{ki}^2 - \omega^2} \tag{3}$$

$$\alpha_i^{\mathrm{V}}(\omega) = \sqrt{\frac{24J_i}{(J_i+1)(2J_i+1)}} \sum_k (-1)^{(J_i+J_k+1)} \left\{ \begin{array}{ccc} J_i & 1 & J_i \\ 1 & J_k & 1 \end{array} \right\} \frac{\omega |\langle \Psi_i \| D \| \Psi_k \rangle|^2}{\Delta E_{ki}^2 - \omega^2} \tag{4}$$

$$\alpha_i^{\mathrm{T}}(\omega) = \sqrt{\frac{40J_i(2J_i-1)}{3(J_i+1)(2J_i+1)(2J_i+3)}} \sum_k (-1)^{(J_i+J_k)} \left\{ \begin{array}{ccc} J_i & 2 & J_i \\ 1 & J_k & 1 \end{array} \right\} \frac{\Delta E_{ki} |\langle \Psi_i \| D \| \Psi_k \rangle|^2}{\Delta E_{ki}^2 - \omega^2} \tag{5}$$

where D is the electric dipole transition operator. It is noted that, when $\omega = 0$, $\alpha_i^{\mathrm{S}}(\omega)$, $\alpha_i^{\mathrm{V}}(\omega)$, and $\alpha_i^{\mathrm{T}}(\omega)$ are referred, respectively, as the static scalar, vector, and tensor polarizabilities for state i. The uncertainties of the polarizabilities are governed by the uncertainties of the reduced transition matrix elements. Under our experimental conditions, the ac Stark shift at the magic wavelength includes the contributions from $\alpha^{\mathrm{S}}_{4s_{1/2}}(\omega)$, $\alpha^{\mathrm{S}}_{3d_{5/2}}(\omega)$, and $\alpha^{\mathrm{T}}_{3d_{5/2}}(\omega)$, and the contribution from $\alpha^{\mathrm{V}}(\omega)$ can be neglected.

Theoretical works [29, 36] show that the contributions from the $4s_{1/2} \rightarrow 4p_{1/2}$ and $4s_{1/2} \rightarrow 4p_{3/2}$ transitions dominate the polarizability of the $4s_{1/2}$ state, and the contributions to the polarizability of the $3d_{5/2}$ state are dominated by the $3d_{5/2} \rightarrow 4p_{3/2}$ transition that constitutes over 88% of the polarizability. Detailed schematic diagram of the energy level transitions can be found in figure 5 in the appendix A. We took the same procedure using the sum-over-states method as in our previous work [29] to calculate the dynamic polarizabilities at the magic wavelength measured here. A set of transition matrix elements were calculated by Dirac–Fock plus core polarization (DFCP) method [29]. 60 B-splines of order $k = 7$ and the radial cutoff $\mathrm{R_{max}} = 250$ a.u. were used. By replacing $\left|\left\langle 4s_{1/2} \| D \| 4p_{1/2} \right\rangle\right|$ and $\left|\left\langle 4s_{1/2} \| D \| 4p_{3/2} \right\rangle\right|$ by the high precision results obtained from the experiment [37], the electric dipole transition matrix elements of $4s_{1/2} \rightarrow np_{1/2,\,3/2}$ $(n = 5-7)$, $3d_{5/2} \rightarrow np_{3/2}$ $(n = 5-7)$, $3d_{5/2} \rightarrow nf_{5/2,\,7/2}$ $(n = 4-6)$ transitions by the results from the relativistic all-order method [36, 38], the matrix element $\left|\left\langle 3d_{5/2} \| D \| 4p_{3/2} \right\rangle\right|$ is extracted to be 3.295(15) a.u.

3.2. BBR shift evaluation

The BBR shift to the $4s_{1/2} \rightarrow 3d_{5/2}$ clock transition frequency can be evaluated according to

$$\Delta_{\mathrm{BBR}}\left(4s_{1/2} \rightarrow 3d_{5/2}\right) = -\frac{1}{2}\left(\alpha_{0,4s_{1/2}} \rightarrow \alpha_{0,3d_{5/2}}\right)(831.9V/m)^2 \left(\frac{T(K)}{300}\right)^4 \tag{6}$$

where α_0 is the static electric-dipole polarizability. Combining the matrix element $\left|\left\langle 3d_{5/2} D 4p_{3/2} \right\rangle\right|$ obtained above and other matrix elements from both experiment and theoretical calculations, the differential static polarizability between the $4s_{1/2}$ and $3d_{5/2}$ states is determined to be $-44.32(32)$ a.u. The corresponding BBR shift at 300 K is 0.3816(28) Hz. Comparing to the existing theoretical values, as listed in table 2, the present value agrees with and slightly better than the best previous theoretical calculation of [36]. The fractional uncertainty of BBR shift can now be updated to be 6.8×10^{-18}. The uncertainty due to the knowledge of the dynamic polarizabilities can be further reduced with the method in [39].

4. Conclusion and perspectives

In summary, we have performed an experimental determination of the infrared magic wavelength in $^{40}Ca^{+}$ with uncertainty less than 0.1 nm. Our result agrees well with theoretical values (DFCP method) but with 1–2 orders of magnitude improvement. By using our measured result, the differential static scalar polarizability has been evaluated as $-44.32(32)$ a.u., also in agreement with the previous theoretical values $-44.3(6)$ a.u but with higher accuracy. The blackbody radiation shift at 300 K has then evaluated as 0.3816(28) Hz, which is also in good agreement with our recent measurement result 0.379 13(12) Hz [31]. It is noted that the infrared magic wavelength for the two Zeeman transitions $|4s^2S_{1/2},\ +1/2\rangle \rightarrow |3d^2D_{5/2},\ +3/2\rangle$ and $|4s^2S_{1/2},\ -1/2\rangle \rightarrow |3d^2D_{5/2},\ -3/2\rangle$ has been predicted theoretically in [29], which has a good agreement with our measurement result in this work. The matrix element of $3d_{5/2} \rightarrow 4f_{7/2}$ transition, whose theoretical

uncertainty is 1.1% using relativistic all-order method, could be extracted and improved from further measurement on this magic wavelength, which can help reduce the BBR shift uncertainty further. Although the differential static scalar polarizability can be experimentally obtained with a better accuracy by measuring the magic RF field [31], it requires that the differential static polarizability of the clock transition is negative [31, 43]. However, many ionic optical clock candidates, such as Yb^+, In^+, and all the atomic optical lattice clock candidates which do not use RF field to trap atoms do not satisfy this criterion. The scheme in this work, which uses the magic wavelength to extract the transition matrix elements, can be an alternative and more general way to determine the differential static polarizability.

Furthermore, the determination of the infrared magic wavelength is also a very important step for building an all-optical trapping ion optical clock in the near future. Long-time all-optical trapping of the ions has already been achieved recently by Schaetz's group [17]. One can trap an ion with optical dipole trap only if the trap potential is higher than the ion kinetic motion energy, and the heating rate of the dipole trap will be higher with relatively near resonance (referred to the Doppler cooling transition $4s^2S_{1/2} \rightarrow 4s^2P_{1/2}$ 397 nm laser) wavelength. The ion lifetime in dipole trap would be a few ms with a few hundreds of GHz red detuning lasers [15, 16]; yet the lifetime can be extended to a few second with a few 100 THz far-off-resonance (also referred to 397 nm) lasers. To realize an ion-based optical clock with all-optical trapping scheme, lifetime of at least 100 ms is required and the heating rate should be maintained as low as possible in order to lower the Doppler and Stark shifts. Building a clock with infrared lasers of hundreds THz of red detuning is a better choice comparing to the 395 nm laser. Besides, one can easily obtain a fiber laser with higher power (>60 W) at the $^{40}Ca^+$ infrared magic wavelength in the range of 1000–1100 nm. The all-optical trapping ion optical clock scheme can be used to trap multiple ions [22], which will potentially increase clock stability. However, the magic wavelength is sensitive to the alignment of the beam and its polarization relative to the magnetic field orientation, in our case, these effects would limit the precision of the magic wavelength to the 0.1 nm level, this would limit the accuracy of the optical clocks. In the practical point of view, building a high accuracy all optical ion clock would require techniques to make the laser pointing and magnetic field more stable.

Data availability statement

All data that support the findings of this study are included within the article (and any supplementary files).

Acknowledgments

Yao Huang, Miao Wang and Zhen Cheng contributed equally to this work. We thank Jun Jiang, Yongbo Tang, Fangfei Wu, V Yudin, A Taichenachev, Zongchao Yan, B Sahoo, and J Ye for help and fruitful discussions. This work is supported by the National Key R&D Program of China (Grants Nos. 2022YFB3904001, 2022YFB3904004 and 2018YFA0307500), the National Natural Science Foundation of China (Grants Nos. 11934014, 12022414, 12121004 and 12174402), the Natural Science Foundation of Hubei Province (Grant No. 2022CFA013), the CAS Youth Innovation Promotion Association (Grants Nos. Y201963 and Y2022099), the CAS Project for Young Scientists in Basic Research (Grant No. YSBR-055), and the Interdisciplinary Cultivation Project of the Innovation Academy for Precision Measurement of Science and Technology (Grant No. S21S2201).

Appendix A. Detailed experimental setup of magic wavelength measurement

A.1. Clock transition laser's locking

Figure 5 shows the relevant energy levels and lasers of $^{40}Ca^+$ optical clock. The $4s^2S_{1/2}$ state is the ground state of the ion, and the $3d^2D$ state is the lowest energy excited state of the ion, which is also a metastable state with a lifetime of about 1 s. The natural linewidth of the corresponding $4s^2S_{1/2} \rightarrow 3d^2D$ transition is approximately 0.16 Hz. For ion's energy level transitions, the two transitions of $4s^2S_{1/2} \rightarrow 3d^2D$ are forbidden transitions, with the upper energy state having a much longer lifetime compared to the upper state of electric dipole transitions $4s^2S_{1/2} \rightarrow 4s^2P$, which makes these transitions ideal for optical clock. The $3d^2D$ state splits into two fine structure sub levels $3d^2D_{3/2}$ and $3d^2D_{5/2}$, which corresponding to the 732 nm and 729 nm lasers to ground state separately, due to spin-orbit coupling. In experiments, the $4s^2S_{1/2} \rightarrow 3d^2D_{5/2}$ transition is chosen as the reference transition for $^{40}Ca^+$ optical clock, and the clock transition laser is 729 nm laser.

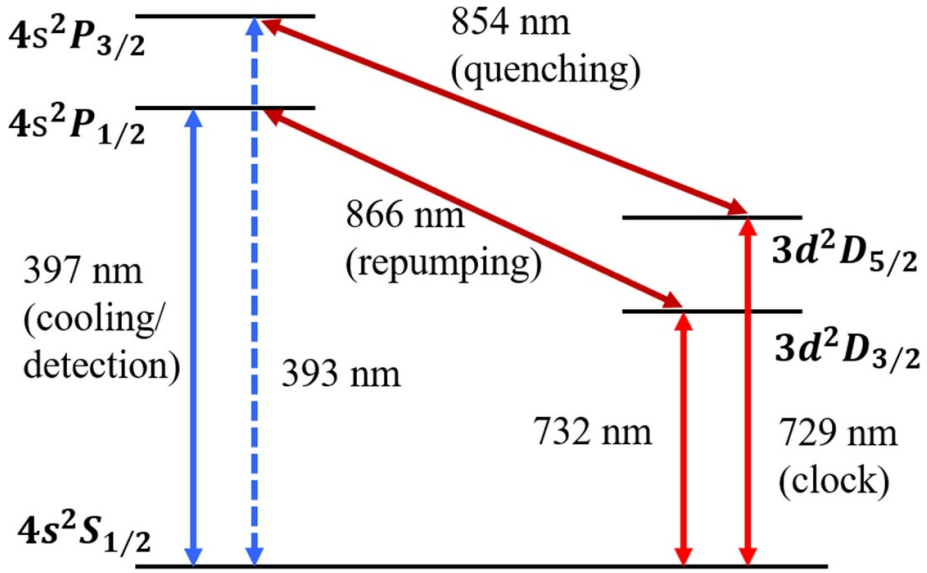

Figure 5. The relevant energy levels and lasers of $^{40}Ca^{+}$ optical clock.

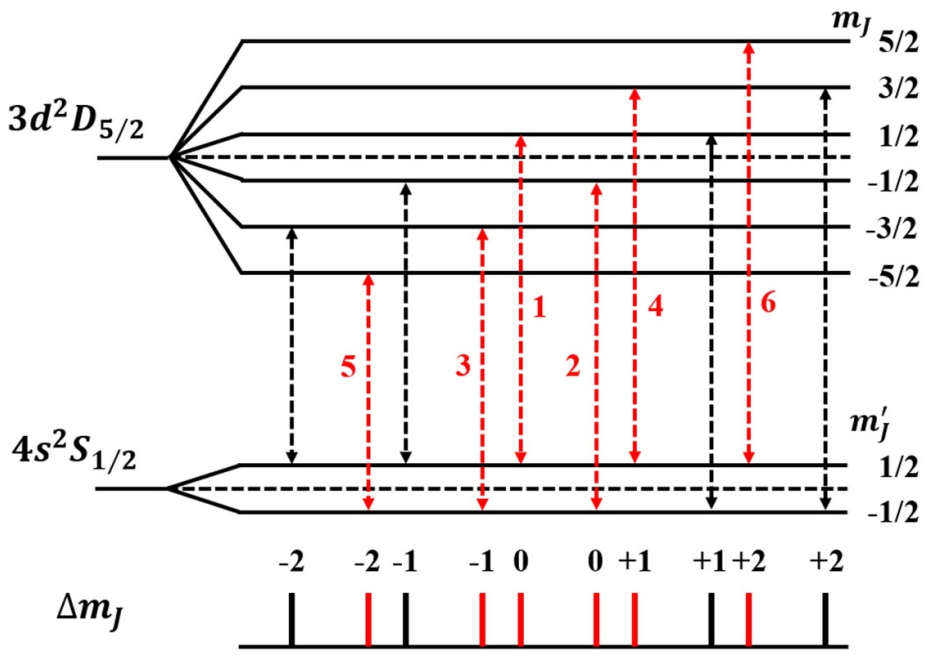

Figure 6. The relevant energy levels and lasers of $^{40}Ca^{+}$ optical clock.

The clock transition $4s^2S_{1/2} \rightarrow 3d^2D_{5/2}$ will split into ten spectral lines in a static magnetic field due to the 1st-order Zeeman effect, as shown in figure 6. Tuning the 729 nm laser's frequency to couple the specific Zeeman component transition is called locking the laser to this Zeeman component transition. Usually, we choose the six set of Zeeman transitions (labeled red in figure 5) to lock the 729 nm laser, and averaged the measured six laser frequencies as the clock transition laser frequency.

A.2. Experimental setup sequence

As illustrated in figure 1, to measure the magic wavelength of clock transition, we need to measure the ac Stark shift caused by the L_m laser with wavelength around 1056 nm. Firstly, a single $^{40}Ca^{+}$ ion is trapped in a miniature ring Paul trap and laser cooled to the temperature of a few mK which correspond to the Doppler cooling loop in figure 5, and the cooling laser 397 nm and repumping laser 866 nm are switched on. Secondly, to measure the magic wavelength, the L_m laser as well as the clock laser which is locked to the Zeeman components of clock transition (which means the frequency of 729 nm is tuned to couple one

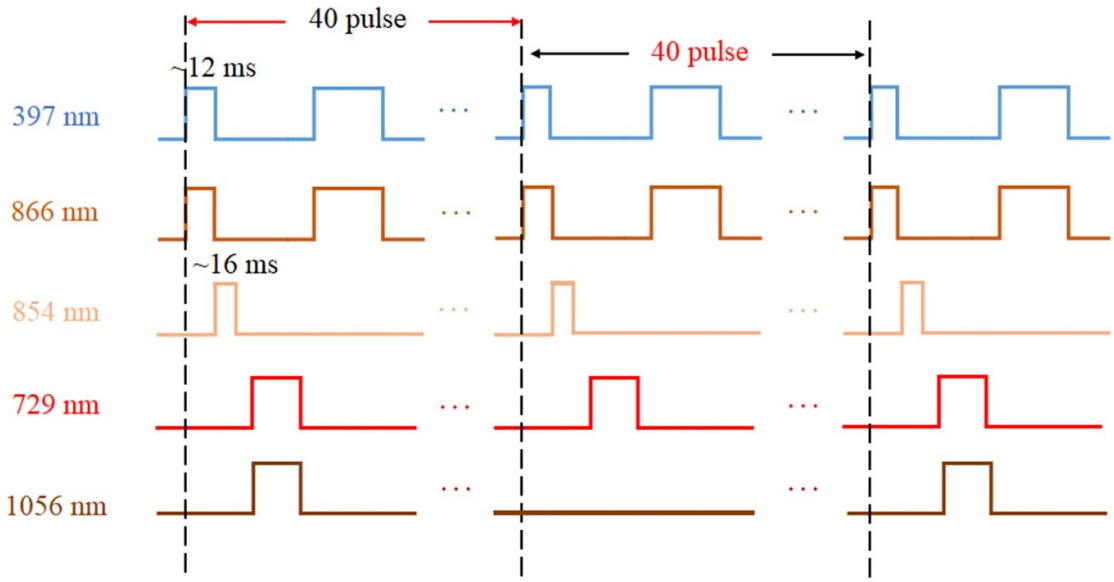

Figure 7. The schematic diagram of the laser pulse of experimental sequence for magic wavelength measurement.

Zeeman transition of $4s^2S_{1/2} \rightarrow 3d^2D_{5/2}$ in figure 6) are switched on, and the quenching laser 854 nm is switched on for a while to prevent the ion from staying in the $3d^2D_{5/2}$ state before the measurement. In this work, we tuned 729 nm to the frequency to drive the two Zeeman transitions: $|4s^2S_{1/2},\ +1/2\rangle \rightarrow |3d^2D_{5/2},\ +3/2\rangle$ and $|4s^2S_{1/2},\ -1/2\rangle \rightarrow |3d^2D_{5/2},\ -3/2\rangle$ as we stated in section 2.3. Then, we measured the clock laser's frequency. Finally, we switched L_m laser off, while the 729 nm clock laser is kept on and tuned to drive the same Zeeman transitions. Then, we measured the clock laser's frequency again. The ac Stark shift caused by the L_m laser is the frequency difference from the two measurement results. The whole experimental sequence is illustrated in figure 7, the two steps of switching the L_m laser on and off alternate with each other for 40 pulses. After the measurement of ac Stark shifts, we obtained the magic wavelength as the zero-crossing of figure 2 as we stated in section 2.3.

Appendix B. Systematic shifts evaluation for the measurement of the infrared magic wavelength

B.1. Broadband laser spectrum

For our detection laser, it is not an absolutely pure monochrome wavelength. We suspect there may be a very small portion of photons with wavelength other than the wavelength measured by the wavemeter, so we took a filter to eliminate the impure portion of the laser spectrum frequency. To evaluate the broad spectral component, two narrow optical bandpass filters (Semrock FF01-1001/234-25) are used to get rid of the spectrum outside the 870–1140 nm range with attenuation of $>10^6$. Then a grating spectrometer is used to analyze the laser spectrum and we found that >99.97% of the laser power is within the wavelength range of 2 nm, only <0.03% of laser power is measured at a wavelength 4 nm shorter. According to our measured relationship between ac Stark shift and the wavelength, <0.03% of laser power at a wavelength 4 nm shorter would shift a magic wavelength measurement by 0.005 nm.

B.2. Background magnetic field drift

The background magnetic field may be changing during the measurements and the fluctuations can be very significant at short times. So, we have added a two-layer magnetic shield around our vacuum chamber. And after that, there is still several μT level fluctuation of magnetic field according to the measurement. Since the measurements is found to be sensitive to the magnetic field direction, the effects of magnetic field change should be considered. In our opinion, the fast fluctuation only caused the broadening of the measured spectrum line shape and did not affect the zero-crossing wavelength of the experiment. While in the other hand, there is still a long-term magnetic field drift during the measurement between different measured data points, which could cause a shift to our measurement. By measuring the compensated magnetic field amplitude (which should be about 0) every few hours, the background magnetic field would only change <30 nT during the whole experiment. The magnetic field amplitude applied is 3800 nT, thus we estimate the parameter θ_p and θ_k would both gain uncertainty of <0.5° due to the background magnetic field change.

According to the relationship between the magic wavelength and those parameters, it would contribute uncertainty of 0.01 nm for θ_p and 0.08 nm for θ_k respectively.

B.3. Other potential sources of systematic shift

There are other potential sources of systematic shift which might be associated with the magic wavelength measurement in our experiment, including the second Doppler shift, the calibration of the wavemeter, etc. The L_m laser could heat the ion or compromise the efficiency of the laser cooling, introducing a second order Doppler shift and Stark shift due to the increase of the ion thermal motion or micromotion. To estimate the second order Doppler shift, we measured the ion temperature by observing the intensity of secular sidebands together with the measurements of the micromotion with RF-photon correlation method, with and without the L_m laser, this effect is measured to be <0.001 nm and is negligible. The L_m laser wavelength after frequency stabilization is monitored by a wavemeter (HighFinesse WS-7) with the absolute accuracy of 100 MHz after the calibration using clock laser, which would cause a measurement uncertainty <0.001 nm, also negligible.

ORCID iDs

Miao Wang https://orcid.org/0000-0003-0734-5880
Zheng Chen https://orcid.org/0000-0003-4864-8271

References

[1] Huang Y, Zhang B, Zeng M, Hao Y, Ma Z, Zhang H, Guan H, Chen Z, Wang M and Gao K 2022 Liquid-nitrogen-cooled Ca^+ optical clock with systematic uncertainty of 3×10^{-18} *Phys. Rev. Appl.* **17** 034041
[2] Huntemann N, Sanner C, Lipphardt B, Tamm C and Peik E 2016 Single-ion atomic clock with 3 x 10^{-18} systematic uncertainty *Phys. Rev. Lett.* **116** 063001
[3] Ushijima I, Takamoto M, Das M, Ohkubo T and Katori H 2015 Cryogenic optical lattice clocks *Nat. Photon.* **9** 185–9
[4] McGrew W F *et al* 2018 Atomic clock performance enabling geodesy below the centimetre level *Nature* **564** 87–90
[5] Bothwell T, Kedar D, Oelker E, Robinson J M, Bromley S L, Tew W L, Ye J and Kennedy C J 2019 JILA SrI optical lattice clock with uncertainty of 2.0×10^{-18} *Metrologia* **56** 065004
[6] Zeng M *et al* 2023 Toward a transportable Ca^+ optical clock with a systematic uncertainty of 4.8×10^{-18} *Phys. Rev. Appl.* **19** 064004
[7] Brewer S M, Chen J-S, Hankin A M, Clements E R, Chou C W, Wineland D J, Hume D B and Leibrandt D R 2019 $^{27}Al^+$ quantum-logic clock with a systematic uncertainty below 10^{-18} *Phys. Rev. Lett.* **123** 033201
[8] Zhiqiang Z, Arnold K J, Kaewuam R and Barrett M D 2023 $^{176}Lu^+$ clock comparison at the 10^{-18} level via correlation spectroscopy *Sci. Adv.* **9** eadg1971
[9] Le Targat R *et al* 2013 Experimental realization of an optical second with strontium lattice clocks *Nat. Commun.* **4** 2109
[10] Huntemann N, Lipphardt B, Tamm C, Gerginov V, Weyers S and Peik E 2014 Improved limit on a temporal variation of mp/me from comparisons of Yb^+ and Cs atomic clocks *Phys. Rev. Lett.* **113** 210802
[11] Safronova M S, Budker D, DeMille D, Kimball D F J, Derevianko A and Clark C W 2018 Search for new physics with atoms and molecules *Rev. Mod. Phys.* **90** 025008
[12] Sanner C, Huntemann N, Lange R, Tamm C, Peik E, Safronova M S and Porsev S G 2019 Optical clock comparison for Lorentz symmetry testing *Nature* **567** 204–8
[13] Lange R, Huntemann N, Rahm J M, Sanner C, Shao H, Lipphardt B, Tamm C, Weyers S and Peik E 2021 Improved limits for violations of local position invariance from atomic clock comparisons *Phys. Rev. Lett.* **126** 011102
[14] Grotti J *et al* 2018 Geodesy and metrology with a transportable optical clock *Nat. Phys.* **14** 437–41
[15] Schneider C, Enderlein M, Huber T and Schaetz T 2010 Optical trapping of an ion *Nat. Photon.* **4** 772–5
[16] Huber T, Lambrecht A, Schmidt J, Karpa L and Schaetz T 2014 A far-off-resonance optical trap for a Ba^+ ion *Nat. Commun.* **5** 5587
[17] Lambrecht A, Schmidt J, Weckesser P, Debatin M, Karpa L and Schaetz T 2017 Long lifetimes and effective isolation of ions in optical and electrostatic traps *Nat. Photon.* **11** 704–7
[18] Arora B, Safronova M S and Clark C W 2011 Tune-out wavelengths of alkali-metal atoms and their applications *Phys. Rev.* A **84** 043401
[19] LeBlanc L J and Thywissen J H 2007 Species-specific optical lattices *Phys. Rev.* A **75** 053612
[20] Herold C D, Vaidya V D, Li X, Rolston S L, Porto J V and Safronova M S 2012 Precision measurement of transition matrix elements via light shift cancellation *Phys. Rev. Lett.* **109** 243003
[21] Holmgren W F, Trubko R, Hromada I and Cronin A D 2012 Measurement of a wavelength of light for which the energy shift for an atom vanishes *Phys. Rev. Lett.* **109** 243004
[22] Schmidt J, Lambrecht A, Weckesser P, Debatin M, Karpa L and Schaetz T 2018 Optical trapping of ion coulomb crystals *Phys. Rev.* X **8** 021028
[23] Derevianko A 2000 Reconciliation of the measurement of parity nonconservation in Cs with the standard model *Phys. Rev. Lett.* **85** 1618–21
[24] Sahoo B K, Chaudhuri R, Das B P and Mukherjee D 2006 Relativistic coupled-cluster theory of atomic parity nonconservation: application to $^{137}Ba^+$ *Phys. Rev. Lett.* **96** 163003
[25] Porsev S G, Beloy K and Derevianko A 2009 Precision determination of electroweak coupling from atomic parity violation and implications for particle physics *Phys. Rev. Lett.* **102** 181601
[26] Liu P L, Huang Y, Bian W, Shao H, Guan H, Tang Y B, Li C B, Mitroy J and Gao K L 2015 Measurement of magic wavelengths for the $^{40}Ca^+$ clock transition *Phys. Rev. Lett.* **114** 223001
[27] Kaur J, Singh S, Arora B and Sahoo B K 2015 Magic wavelengths in the alkaline-earth-metal ions *Phys. Rev.* A **92** 031402

[28] Jiang J, Jiang L, Wang X, Zhang D-H, Xie L-Y and Dong C-Z 2017 Magic wavelengths of the Ca^+ ion for circularly polarized light *Phys. Rev.* A **96** 042503
[29] Tang Y-B, Qiao H-X, Shi T-Y and Mitroy J 2013 Dynamic polarizabilities for the low-lying states of Ca^+ *Phys. Rev.* A **87** 042517
[30] Haycock D L, Hamann S E, Klose G and Jessen P S 1997 Atom trapping in deeply bound states of a far-off-resonance optical lattice *Phys. Rev.* A **55** R3991–4
[31] Huang Y, Guan H, Zeng M, Tang L and Gao K 2019 $^{40}Ca^+$ ion optical clock with micromotion-induced shifts below 1×10^{-18} *Phys. Rev.* A **99** 011401
[32] Jiang J, Jiang L, Wu Z W, Zhang D-H, Xie L-Y and Dong C-Z 2019 Angle-dependent magic wavelengths for the $4s_{1/2} \rightarrow 3d_{5/2,3/2}$ transitions of Ca^+ ions *Phys. Rev.* A **99** 032510
[33] Manakov N L, Ovsiannikov V D and Rapoport L P 1986 Atoms in a laser field *Phys. Rep.* **141** 320–433
[34] Beloy K 2009 *Theory of the Ac Stark Effect on the Atomic Hyperfine Structure and Applications to Microwave Atomic Clocks* (University of Nevada)
[35] Le Kien F, Schneeweiss P and Rauschenbeutel A 2013 Dynamical polarizability of atoms in arbitrary light fields: general theory and application to cesium *Eur. Phys. J.* D **67** 1–16
[36] Safronova M S and Safronova U I 2011 Blackbody radiation shift, multipole polarizabilities, oscillator strengths, lifetimes, hyperfine constants, and excitation energies in Ca^+ *Phys. Rev.* A **83** 012503
[37] Hettrich M, Ruster T, Kaufmann H, Roos C F, Schmiegelow C T, Schmidt-Kaler F and Poschinger U G 2015 Measurement of dipole matrix elements with a single trapped ion *Phys. Rev. Lett.* **115** 143003
[38] Kaur J, Singh S, Arora B and Sahoo B K 2017 Annexing magic and tune-out wavelengths to the clock transitions of the alkaline-earth-metal ions *Phys. Rev.* A **95** 042501
[39] Barrett M D, Arnold K J and Safronova M S 2019 Polarizability assessments of ion-based optical clocks *Phys. Rev.* A **100** 043418
[40] Sahoo B K, Das B P and Mukherjee D 2009 Relativistic coupled-cluster studies of ionization potentials, lifetimes, and polarizabilities in singly ionized calcium *Phys. Rev.* A **79** 052511
[41] Arora B and Safronova M S 2007 Blackbody-radiation shift in a $^{43}Ca^+$ ion optical frequency standard *Phys. Rev.* A **76** 064501
[42] Mitroy J and Zhang J Y 2008 Long range interactions of the Mg^+ and Ca^+ ions *Eur. Phys. J.* D **46** 415–24
[43] Dubé P, Madej A A, Tibbo M and Bernard J E 2014 High-accuracy measurement of the differential scalar polarizability of a $^{88}Sr^+$ clock using the time-dilation effect *Phys. Rev. Lett.* **112** 173002